Nanoscale

PAPER

Published on 05 February 2016
Licence and permissions

Cite this: *Nanoscale*, 2016, **8**, 6057

Nano-scale polar–nonpolar oxide heterostructures for photocatalysis†

Hongli Guo,[a,b] Wissam A. Saidi,[c] Jinlong Yang[a,b] and Jin Zhao*[a,b,d]

Received 7th December 2015,
Accepted 5th February 2016

DOI: 10.1039/c5nr08689b

www.rsc.org/nanoscale

We proposed based on first principles density functional theory calculations that a nano-scale thin film based on a polar–nonpolar transition-metal oxide heterostructure can be used as a highly-efficient photocatalyst. This is demonstrated using a $SrTiO_3/LaAlO_3/SrTiO_3$ sandwich-like heterostructure with photocatalytic activity in the near-infrared region. The effect of the polar nature of $LaAlO_3$ is two-fold. First, the induced electrostatic field accelerates the photo-generated electrons and holes into opposite directions and minimizes their recombination rates. Hence, the reduction and oxidation reactions can be instigated at the $SrTiO_3$ surfaces located on the opposite sides of the heterostructure. Second, the electric field reduces the band gap of the system making it photoactive in the infrared region. We also show that charge separation can be enhanced by using compressive strain engineering that creates ferroelectric instability in STO. The proposed setup is ideal for tandem oxide photocatalysts especially when combined with photoactive polar materials.

Introduction

By directly converting light to chemical fuels, photoelectrochemical cells (PECs) hold great promise for making solar power meet our future energy needs. The catalytic reactions in PECs are instigated by photogenerated holes and electrons after light illumination on a photosensitive material. The generated holes are responsible for initiating the oxidation pathway while the electrons are responsible for initiating the reduction reactions.

The main issues in conventional PECs are the low efficiency of solar energy conversion in addition to the high cost and device longevity. The light conversion efficiency is mainly determined by three factors. The first factor is related to the light absorption efficiency to generate electron–hole pairs, which could be increased using semiconductors with a band gap <2 eV. This is because the energy of the solar spectrum is roughly 44% visible light (1.3–2.1 eV), 48% infrared, and 8% ultraviolet. Standard photocatalytic materials such as TiO_2 have a large band gap (>3 eV).[1–3] To reduce the TiO_2 band gap and improve visible light absorption, several schemes are investigated for band engineering such as using cation or anion (co)doping, and synthesizing nano-crystals but with only limited success.[4–10] The second factor that limits the PEC efficiency is the recombination rates of the generated charge carriers, which can be significantly alleviated by breaking the translational symmetry between the generated holes and electrons. This can be achieved, *e.g.*, by using an external field that couples to the charge of the photo-induced carriers as in an n–p junction that is typically used in conventional semiconductor PECs. Other novel approaches to minimize recombination rates such as using a ferroelectric material or advanced heterostructures are also currently being investigated.[11,12] Finally, the last factor that determines the PEC performance is associated with the efficiency of chemical reactions that are instigated by the photo-induced charge carriers. To date, successful materials that are particularly employed in conventional photocatalysts include metal oxides such as TiO_2 and $SrTiO_3$ (STO).[13–20] The major challenge in PEC optimization is in designing photochemical cells that can successfully circumvent all of these limitations.

Here, we study the photocatalytic reactivity of nanocapacitor-like heterostructures by inspecting their electronic structure and optical properties using first principles calculations. Our results imply that this material can be a candidate for a new photocatalyst. Namely, the proposed nano structure combines two ultrathin oxide films that act as photo-cathode and -anode materials, and a polar material with an intrinsic

[a]*ICQD/Hefei National Laboratory for Physical Sciences at Microscale, and Key Laboratory of Strongly-Coupled Quantum Matter Physics, Chinese Academy of Sciences, and Department of Physics, University of Science and Technology of China, Hefei, Anhui 230026, China*
[b]*Synergetic Innovation Center of Quantum Information & Quantum Physics, University of Science and Technology of China, Hefei, Anhui 230026, China*
[c]*Department of Mechanical Engineering and Materials Science, University of Pittsburgh, Pittsburgh, Pennsylvania 15261, USA*
[d]*Department of Physics, University of Pittsburgh, Pittsburgh, Pennsylvania 15261, USA. E-mail: zhaojin@ustc.edu.cn*
†Electronic supplementary information (ESI) available. See DOI: 10.1039/c5nr08689b

electric field that breaks translational symmetry and inhibits carrier recombination rates. The decrease in the band gap of the system, mainly in the interface region between the polar and non-polar materials, improves substantially the absorption in the near-infrared to visible light regions. We demonstrate the properties of this heterostructure based on STO and $LaAlO_3$ (LAO), as shown in the schematic of Fig. 1. Additionally, we show that compressive strain can polarize the STO layers inducing an electric field in the whole heterostructure, which enhances charge separation even with thicker STO slabs.

Heterostructures composed of perovskite oxides such as STO and LAO, epitaxially stacked along the (001) direction have generated a lot of interest in recent years.[21–25] The exciting properties stem from the polar–non-polar nature of STO/LAO as can be seen by examining the nominal charges of the layers, which are +1 (LaO) and −1 (AlO_2) in LAO (001) layers, and neutral for the TiO_2 and SrO layers of STO (001). Hence in LAO (001)/STO(001) heterostructures there are two possible interfaces, namely n-type $(LaO)^+/(TiO_2)^0$ and p-type $(AlO_2)^-/(SrO)^0$. Further, the charge modulation in LAO results in the buildup of a voltage that is nearly proportional to the number of LAO layers and thus diverges linearly with the LAO thickness. This leads to a "polar catastrophe" that can be avoided by transfer of half an electron (hole) per 2D unitcell across the n-type (p-type) interface.[26]

The nanocapacitor-like STO/LAO/STO heterostructure has an n-type interface on one side and a p-type interface on the other, as shown in Fig. 1. This ensures the existence of an unidirectional electric field in the polar LAO region. The macroscopic electric field in LAO increases the local energy as shown in Fig. 1 such as the energy gap of the entire system is determined by the difference between the CBM of STO on the left and VBM of STO on the right. As the LAO thickness increases, the voltage across LAO increases as well leading to the decrease of the band gap of the system and inducing an insulator-to-metal transition at a critical thickness of LAO. Here the buildup of the electric field in the polar LAO material has two main effects on the properties of the heterostructure especially when applied as a PEC. First, the electric field decreases the band gap of the STO/LAO/STO heterostructure, and we show that this enhances the absorption efficiency in the infrared. Second, the intrinsic electric field in LAO breaks the translational symmetry and inhibits the recombination rates. Further, by using ultrathin STO films, photogenerated charges can instigate surface reactions at the bottom and top STO surfaces.

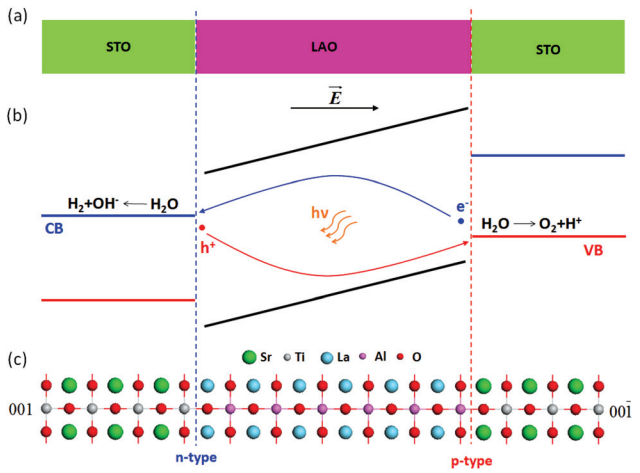

Fig. 1 The schematic and atomic structure of the n–p type STO/LAO/STO (001) heterostructure.

Results and discussion

We first determine the band gap of the STO/LAO/STO heterostructure. Here, the interface region between STO and LAO is n–p with $(LaO)^+/(TiO_2)^0$ on the right side of the junction and $(AlO_2)^-/(SrO)^0$ on the left side, as shown in Fig. 1. Because of two possible terminations SrO and TiO_2 of the STO (001) surface, there are four possible heterostructures depending on the STO surface layer, namely SrO–SrO, SrO–TiO_2, TiO_2–SrO, and TiO_2–TiO_2. We use 1–2 unitcells (ucs) of STO overlayers respectively, as shown in Fig. 2(a). Because the thickness of LAO is an important factor that controls the electronic band structure of the interface,[27–29] we have additionally investigated the heterostructures for different LAO thicknesses. Fig. 2 (b and c) show that the band gap decreases as the LAO thickness increases, which is similar to the case of STO/LAO.[30] Also, in agreement with STO/LAO,[30] we find that STO/LAO/STO has an indirect band gap (see the ESI†), which closes after a critical thickness with a concurrent charge transfer from the VB to CB. As seen in Fig. 2, the critical thickness is the smallest for the TiO_2–TiO_2 system (3uc) and the largest for the SrO–SrO system

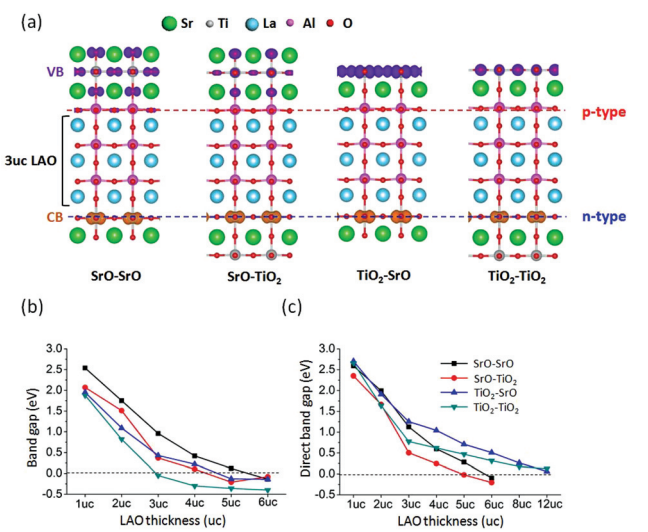

Fig. 2 (a) The atomic structure of n–p-type STO/LAO/STO heterostructures with 3uc LAO and different STO terminations together with the orbital spatial distribution of the VB and CB at the Γ point. (b) and (c) The thickness dependence of the indirect and direct band gap of STO/LAO/STO with different terminations.

This journal is © The Royal Society of Chemistry 2016

(6uc). From the schematic map in Fig. 1, the band gap of n–p type STO/LAO/STO is determined by the band alignment of the two STO layers and can be estimated as $E_{gap} = E_{gap_STO} - \Delta V_{LAO}$, where E_{gap_STO} is the band gap of STO and ΔV_{LAO} is the electrostatic potential induced by polarized LAO. ΔV_{LAO} depends on the LAO thickness. One can see that before the charge transfer from the VB to CB, E_{gap} decreases almost linearly with the LAO thickness, which is consistent with previous first-principles calculations.[30] After the closing of the bandgap, the charge transfer from the VB to CB balances the increasing electrostatic potential. As shown in Fig. 2(a), the VB and CB, which are the hole and electron acceptor bands, are mainly localized on the (001) and (00$\bar{1}$) surfaces respectively because of the built-in electrostatic field. The VB is mainly due to the oxygen p-band of oxygen while the CB is due to the Ti d-bands, which contributes to the 2D electron gas at the interface, as reported previously[30,31]

The built-in electrostatic field can be directly observed in the layer resolved density of states (DOS) shown in Fig. 3. Here for a better description of the band structure we used the screened hybrid functional HSE06.[75] We show the DOS for the four STO/LAO/STO heterostructures with different terminations, and with only 3ucs LAO. The nearly termination-independent rigid shift of DOS of each layer in energy clearly shows the existence of a built-in electrostatic field, which can accelerate the electrons and holes into opposite directions, making the (001) and (00$\bar{1}$) surfaces electron and hole doped, respectively.

One key factor for photocatalytic water splitting is the electron transfer between the photocatalyst and the water redox species. Thermodynamically, this transfer takes place with a proper band alignment at which the conduction band minimum (CBM) of the p-type photocathode is more negative in potential than the water reduction potential V_{H^+/H_2}, and the valence band maximum (VBM) of the n-type photocathode is more positive in potential than the water oxidation potential

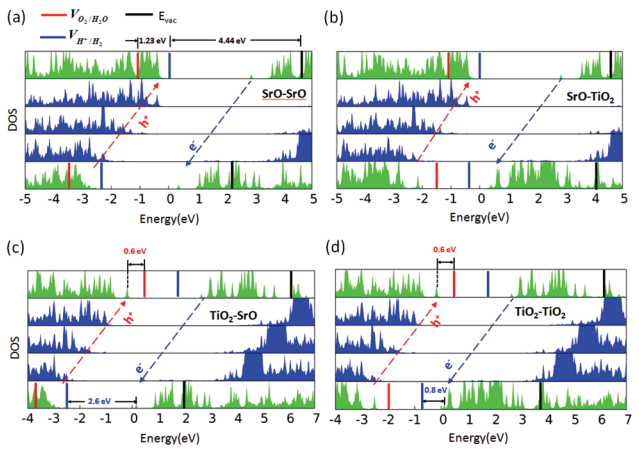

Fig. 3 DOS of four n–p-type STO/LAO/STO heterostructures with 3uc LAO and different STO terminations. The redox potentials of H_2O are marked by the blue and red lines. The E_{vac} of the two opposite sides are marked using black lines. Oxidation and reduction powers for TiO_2–SrO and TiO_2–TiO_2 systems are also marked.

V_{O_2/H_2O}, which can be obtained from the half reactions $2H^+ + 2e^- \leftrightarrow H_2$ (V_{H^+/H_2}) and $O_2 + 4H^+ + 4e^- \leftrightarrow 2H_2O$ (V_{O_2/H_2O}).[32] In principle, the H_2O redox potentials can be calculated by the molecular dynamics simulation or the mean-field approximation considering the interaction between the liquid–solid interface.[33–35] However, this is beyond the scope of this work and we use instead the experimental values.[32] Similar band alignment analysis was applied before for semiconductors as well as for the newly developed two-dimensional nano materials.[36,37] In our study, we use the HSE functional to get a more accurate band alignment to the vacuum level in the system, at least compared to local and semi-local functionals (see Fig. S1 in the ESI†). The results are summarized in Fig. 3 where V_{O_2/H_2O} and V_{H^+/H_2} are shifted by the vacuum potential (E_{vac}) and the Fermi energy is set to zero. One can see that E_{vac} of the opposite sides are determined by the terminations and aligned by the electric field in LAO.

The oxidation (reduction) power of the photocatalyst is defined as the energy difference between V_{O_2/H_2O}(V_{H^+/H_2}) and the VBM (CBM) level of the material. From Fig. 3, we see that SrO–SrO and SrO–TiO_2 heterostructures can be only used for H_2O reduction. This is because V_{H^+/H_2} is located below CBM that thermodynamically favors charge transfer, while V_{O_2/H_2O} is above VBM and thus charge transfer is inhibited. On the other hand, TiO_2–TiO_2 and TiO_2–SrO heterostructures can be used for both H_2O reduction and oxidation as the water redox potentials fall in the bandgap of the system. As seen from the figure, the oxidation and reduction powers for these heterostructures are respectively 0.8 and 0.6 eV for TiO_2–TiO_2 termination, and 0.6 and 2.6 eV for the TiO_2–SrO termination. The nearly balanced oxidation/reduction powers for the TiO_2–TiO_2 heterostructure is expected to minimize the difference between the reduction and oxidation reactions, and thus can potentially improve the photocatalytic efficiency. The large reduction potential for TiO_2–SrO termination is also of interest as the main purpose of the photocatalytic reaction is to obtain hydrogen gas. The energy alignment with respect to H_2O redox potentials are only shown for the 3uc LAO heterostructure, nevertheless the band alignments are very close to other structures with different thicknesses, and hence our conclusions are independent of the LAO thickness (see the ESI, Fig. S5†). In addition, the band alignment of TiO_2–TiO_2 heterostructures is very similar to the STO slab with TiO_2 termination (Fig. S1†). These results show that the band alignment mainly depends on the termination, and is unlikely to be affected by the electric field in LAO. Therefore although here we only calculate the band alignment in a vacuum, we expected that the n–p type STO/LAO/STO works similar to STO for H_2O oxidation and reduction in a real photocatalytic system.[37]

The optimum band alignment of the STO/LAO/STO heterostructure with respect to the water redox potentials is required for the PEC. However, the efficiency of this heterostructure as a photocatalyst depends also on its ability to absorb light. This can be gauged by examining the complex dielectric function $\varepsilon(\omega) = \varepsilon_1(\omega) + i\varepsilon_2(\omega)$ computed through momentum representation from the overlap matrix elements between occupied and

unoccupied eigenstates.[38] For better accuracy, we employed the HSE functional in this calculation. Using $\varepsilon(\omega)$ the absorption coefficient, $\alpha(E)$, is determined from the following expression (see the ESI†):

$$\alpha(E) = \frac{4\pi e}{hc}\left\{\frac{[\varepsilon_1{}^2 + \varepsilon_2{}^2]^{1/2} - \varepsilon_1}{2}\right\}^{1/2}.$$

Fig. 4(a) shows $\alpha(E)$, of STO/LAO/STO with different terminations for the case of 5ucs of LAO. In comparison with the absorption spectrum of bulk $SrTiO_3$ (shown in Fig. S4†), besides the absorption in the ultraviolet region, all of the heterostructures have an additional absorption peak in the range 0.2–0.5 eV when the LAO thickness exceeds 3–4 unit cells. This low-energy peak results from the band gap closing of the whole system and ensures light adsorption in the infrared region. The absorption in the ultraviolet region generates electron hole pairs within STO, which can be separated by the built-in electric field over LAO as schematically shown by the arrows in Fig. 3. Simultaneously, the absorption in the infrared to visible light region can generate the separated electrons and holes directly. Comparing the 4 different terminations of the heterostructures, we found the absorption intensity mainly depends on the direct band gap. Here, although TiO_2–TiO_2 has the smallest in-direct band gap, it has a relatively weak absorption, which can be understood from its relatively large direct band gap as shown in Fig. 2(c). See Fig. S2 and Table S1† for more information. Fig. 4(b) and (c) show the absorption intensity for TiO_2–TiO_2 and TiO_2–SrO heterostructures, which can be used for both H_2O reduction and oxidation as shown before. One can see that the absorption intensity increases with thicker LAO slabs because of the decrease in the direct bandgap. We also investigated the effects of the STO thickness and showed that the absorption intensity is insensitive to its thickness. This is shown in Fig. 4(d) for the TiO_2–TiO_2 heterostructure with 6ucs of LAO and 1, 3, and 5ucs of STO. This finding is encouraging because we expect that the heterostructures will have enhanced catalytic efficiency with ultrathin STO slabs.

The requirement for ultrathin STO layers can be alleviated using strain engineering. It has been previously shown that compressive strain can induce a ferroelectric instability in STO.[39] Thus, by tuning the in-plane lattice constant, it is expected that the heterostructures can be designed to have a macroscopic electric field in the LAO and STO layers that drives the photo-generated charge carriers in opposite directions. We demonstrated this for the n–p STO/LAO/STO heterostructure using a 3% compressive strain with an in-plane lattice constant of 3.78 Å. Fig. 5 shows the resulting projected layer DOS obtained using HSE06 as described before. The energy shift of the VB in the STO and LAO layers indicates that the heterostructure supports as a whole a polarization field, and not only in the LAO region as in the unstrained case shown in Fig. 3. We showed that with the strained case, the heterostructure can also have a large absorption coefficient $\alpha(E)$ in the infrared region (see Fig. S5†), and thus the system remains photocatalytically active as in the unstrained case. In addition to the effect of the electric field on charge separation, the polarization of the system is expected to improve on the band alignment with the water redox potentials as was demonstrated on TiO_2 supported on a ferroelectric STO system.[40]

By studying the n–p-type STO/LAO/STO heterostructure as an example, we demonstrate a new perspective of oxide heterostructure applications in photocatalysis as a nanosize PEC. The crucial factor here is the polar nature of LAO, which increases the light absorption in the infrared region and effectively separates the generated charge carriers. There have been active debates about the existence of the electric field in LAO.[25,41–63] The internal electrostatic field in LAO could be

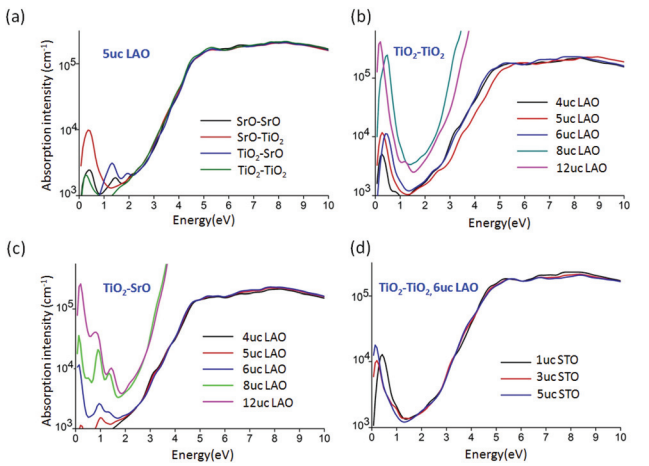

Fig. 4 The absorption intensity of different STO/LAO/STO heterostructures. (a) STO/LAO/STO heterostructures with 5uc LAO and different terminations. (b) and (c) TiO_2–TiO_2 and TiO_2–SrO heterostructures with different LAO thicknesses. (d) The TiO_2–TiO_2 heterostructure with different STO thicknesses.

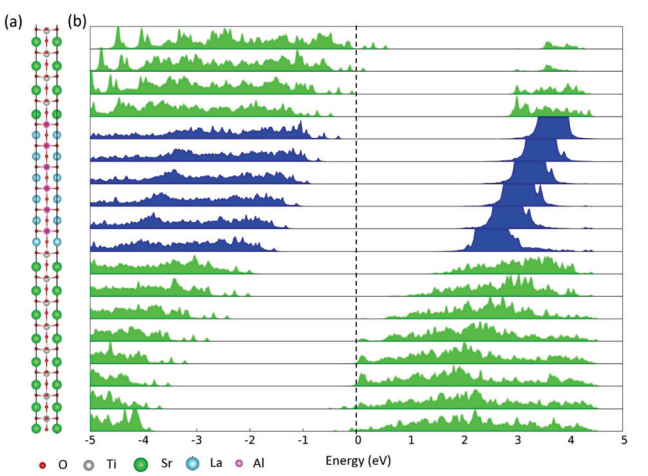

Fig. 5 (a) Configuration of optimized TiO_2–SrO type 4ucs STO/6ucs LAO/8ucs STO heterostructures. (b) The DOS of n–p-type STO/LAO/STO heterostructures with imposed 3% compressive strain.

This journal is © The Royal Society of Chemistry 2016

affected by oxygen defects and interface inter-mixing in the oxides.[41,47,56,59,62] However, there have been several direct and indirect evidence supporting the existence of a built-in electric field,[42,44,51,52,54,57,60,61] For example, experimental and computational studies showed that the internal electric field in LAO/STO/Au can be as large as 80 mV $Å^{-1}$.[51] (See the ESI† for more details.) Additionally, we showed that by using a compressive strain, STO can also be polar, and thus charge separation in STO/LAO/STO will be enhanced even with thick STO layers. In this report, we show the internal electric field that can enhance the charge separation, the photo-generated electron/hole dynamics to show the process of charge carrier separation and being trapped by the adsorbed molecules is an interesting topic for future investigation, but beyond the scope of the current work.

It is known that oxygen evolution reaction is one of the most important factors for H_2O splitting. A recent study of H_2O oxidation on TiO_2 supported on a ferroelectric STO demonstrated that the electric field in strained STO also helps to reduce the thermodynamic barriers and improve the reaction efficiency.[40] We expect that the electric field in LAO in the n–p-type STO/LAO/STO nanostructure has similar effects and we plan to investigate it in our future work.

Recently, Li *et al.* proposed a metal-free photocatalyst based on a BN bilayer decorated with F and H atoms on two sides of the BN layer, which is also found to be active for near-infrared light.[64] This has some similarities with our proposed model except that in our case STO is used as a support for the photocatalyst, which is expected to be advantageous because the exposed STO is a well-known photocatalyst. Additionally, the oxides are amenable to a diverse array of techniques for enhancing their catalytic activity such as by depositing noble metal cluster and cation (co)doping.[65] Finally, the STO/LAO heterostructure with an atomic sharp surface and interface has been synthesized using pulsed laser deposition (PLD) and molecular beam epitaxy (MBE) techniques. Using such techniques, the thickness of LAO can be controlled precisely.[30]

Another advantage of oxide heterostructures is that we can flexibly combine different polar non-polar oxides. For example, it is possible to replace STO by TiO_2. As reported by Kennedy *et al.*,[66] anatase TiO_2 (001) can be grown on LAO and STO substrates. The photocatalysis efficiency might be improved because of the high surface reactivity of anatase TiO_2(001).[67] Also, as a widely used photocatalyst, TiO_2 works well under the acidic and the oxidative conditions. We have determined the electronic structure and photo-absorption properties of n–p type TiO_2/LAO/TiO_2 (001) (Fig. S7† shows the structure and absorption spectra), and they are similar to the STO/LAO/STO heterostructure. The non-polar STO or TiO_2 is also possible to be combined with another polar metal oxide, for example $LaVO_3$ or $GdTiO_3$.[68,69] With different polar metal oxides, the internal electrostatic field can be different. Additionally, by using a polar material with a small band gap like $LaVO_3$, the absorption efficiency can be increased substantially because in this case photocarriers can be generated in the bulk polar region[11] in addition to the interfacial region between the polar and non-polar materials. By tuning this factor, it is possible to design tandem oxide heterostructure photocatalysts active for light absorption with different wavelengths. We expect that the facility of growing oxide heterostructures, together with our proposed model, will enable the discovery of new photocatalysts with high efficiency.

Conclusions

In summary, we propose that nanocapacitor-like heterostructures based on non-polar and polar oxides can be used as an efficient photocatalytic material. The proposed heterostructure combines two ultrathin oxide films which act as photocathode and -anode materials, and a polar material with an intrinsic internal electric field which enhances the charge carrier separation and reduces the band gap. The decrease in the band gap of the system improves substantially the absorption in the near-infrared to visible light regions. We demonstrate these properties based on first principles calculations of n–p type STO/LAO/STO. Additionally, we show that compressive strain can polarize the STO layers inducing an electric field in all of the heterostructure, which enhances charge separation even with thicker STO slabs. This design can also be used for other combinations of oxide heterostructures to accommodate diverse requirements.

Computational method

The proposed photocatalytic properties are elucidated using first-principles density functional theory (DFT) calculations, as implemented in VASP.[70] The ion-electron interactions are described by the projector-augmented wave method.[71] We used the generalized gradient approximation (GGA) with PBE functional.[72] Static local electronic correlations are added to the GGA exchange correlation potential in the GGA + U method with U = 10 eV and J = 0.64 eV (Ti_{3d}).[73] Using these U and J values, the obtained band gap of bulk $SrTiO_3$ is 3.19 eV that is in excellent agreement with the experimental value.[74] To further validate the GGA + U calculations, we use the screened hybrid functional HSE06[75] to obtain more accurate band structures and alignments of the heterostructures.[76] We used a Monkhorst–Pack grid of (7 × 7 × 1) k-points and 400 eV energy cutoff for the structure optimization, and (9 × 9 × 1) and 500 eV cutoff for the electronic structure calculation. In order to avoid interactions between the neighboring slabs, 15 Å of vacuum is inserted between the neighboring slabs along the non-periodic direction, in conjunction with the dipole correction.[77] In our calculations, all of the atomic positions are relaxed until the force on each atom is less than 0.05 eV $Å^{-1}$. The lattice constants of LAO and STO are 3.789 and 3.905 Å and there is 2.9% lattice mismatch.[25] We used the experimental lattice constant of STO 3.905 Å to fix the in-plane lattice constant of the heterostructure.

Acknowledgements

This work is supported by NSFC (21373190, 11322434, 21421063), by the National Key Basic Research Program (2011CB921404). WAS acknowledges a startup fund from the University of Pittsburgh. Calculations were performed at the Shanghai Supercomputer Center and Environmental Molecular Sciences Laboratory at the PNNL, a user facility sponsored by the DOE Office of Biological and Environmental Research.

Notes and references

1 A. F. a. K. Honda, *Nature*, 1972, **238**, 37–38.
2 R. Asahi, T. Morikawa, T. Ohwaki, K. Aoki and Y. Taga, *Science*, 2001, **293**, 269–271.
3 A. Fujishima, T. N. Rao and D. A. Tryk, *J. Photochem. Photobiol., C*, 2000, **1**, 1–21.
4 H.-C. Chen, C.-W. Huang, J. C. Wu and S.-T. Lin, *J. Phys. Chem. C*, 2012, **116**, 7897–7903.
5 Q. Fu, T. He, J. Li and G. Yang, *J. Appl. Phys.*, 2012, **112**, 104322.
6 A. Kudo, R. Niishiro, A. Iwase and H. Kato, *Chem. Phys.*, 2007, **339**, 104–110.
7 C. P. Cheney, P. Vilmercati, E. W. Martin, M. Chiodi, L. Gavioli, M. Regmi, G. Eres, T. A. Callcott, H. H. Weitering and N. Mannella, *Phys. Rev. Lett.*, 2014, **112**, 5.
8 Y. Gai, J. Li, S.-S. Li, J.-B. Xia and S.-H. Wei, *Phys. Rev. Lett.*, 2009, **102**, 036402.
9 Y. Wang, Z. Cheng, S. Tan, X. Shao, B. Wang and J. Hou, *Surf. Sci.*, 2013, **616**, 93–99.
10 C. P. Cheney, P. Vilmercati, E. Martin, M. Chiodi, L. Gavioli, M. Regmi, G. Eres, T. Callcott, H. H. Weitering and N. Mannella, *Phys. Rev. Lett.*, 2014, **112**, 036404.
11 E. Assmann, P. Blaha, R. Laskowski, K. Held, S. Okamoto and G. Sangiovanni, *Phys. Rev. Lett.*, 2013, **110**, 078701.
12 H. Liang, L. Cheng, X. Zhai, N. Pan, H. Guo, J. Zhao, H. Zhang, L. Li, X. Zhang and X. Wang, *Sci. Rep.*, 2013, **3**, 1975.
13 K. Domen, A. Kudo, T. Onishi, N. Kosugi and H. Kuroda, *J. Phys. Chem.*, 1986, **90**, 292–295.
14 K. Domen, S. Naito, T. Onishi, K. Tamaru and M. Soma, *J. Phys. Chem.*, 1982, **86**, 3657–3661.
15 M. Miyauchi, A. Nakajima, A. Fujishima, K. Hashimoto and T. Watanabe, *Chem. Mater.*, 2000, **12**, 3–5.
16 R. Niishiro, H. Kato and A. Kudo, *Phys. Chem. Chem. Phys.*, 2005, **7**, 2241–2245.
17 S. Ouyang, H. Tong, N. Umezawa, J. Cao, P. Li, Y. Bi, Y. Zhang and J. Ye, *J. Am. Chem. Soc.*, 2012, **134**, 1974–1977.
18 X. Zhang, K. Huo, L. Hu, Z. Wu and P. K. Chu, *J. Am. Ceram. Soc.*, 2010, **93**, 2771–2778.
19 U. Diebold, N. Ruzycki, G. S. Herman and A. Selloni, *Catal. Today*, 2003, **85**, 93–100.
20 M. A. Henderson, *Surf. Sci.*, 2012, **606**, 505–509.
21 M. B. Shalom, M. Sachs, D. Rakhmilevitch, A. Palevski and Y. Dagan, *Phys. Rev. Lett.*, 2010, **104**, 126802.
22 J. A. Bert, B. Kalisky, C. Bell, M. Kim, Y. Hikita, H. Y. Hwang and K. A. Moler, *Nat. Phys.*, 2011, **7**, 767–771.
23 J.-S. Lee, Y. Xie, H. Sato, C. Bell, Y. Hikita, H. Hwang and C.-C. Kao, *Nat. Mater.*, 2013, **12**, 703–706.
24 Y. Xie, C. Bell, T. Yajima, Y. Hikita and H. Y. Hwang, *Nano Lett.*, 2010, **10**, 2588–2591.
25 A. Ohtomo and H. Hwang, *Nature*, 2004, **427**, 423–426.
26 N. Nakagawa, H. Y. Hwang and D. A. Muller, *Nat. Mater.*, 2006, **5**, 204–209.
27 S. Thiel, G. Hammerl, A. Schmehl, C. Schneider and J. Mannhart, *Science*, 2006, **313**, 1942–1945.
28 M. Huijben, G. Rijnders, D. H. Blank, S. Bals, S. Van Aert, J. Verbeeck, G. Van Tendeloo, A. Brinkman and H. Hilgenkamp, *Nat. Mater.*, 2006, **5**, 556–560.
29 R. Pentcheva and W. E. Pickett, *Phys. Rev. Lett.*, 2009, **102**, 107602.
30 W.-j. Son, E. Cho, B. Lee, J. Lee and S. Han, *Phys. Rev. B: Condens. Matter*, 2009, **79**, 245411.
31 Z. S. Popović, S. Satpathy and R. M. Martin, *Phys. Rev. Lett.*, 2008, **101**, 256801.
32 A. J. Nozik, *Annu. Rev. Phys. Chem.*, 1978, **29**, 189–222.
33 A. Kovalenko and F. Hirata, *J. Chem. Phys.*, 1999, **110**, 10095–10112.
34 J. Rossmeisl, E. Skulason, M. E. Bjorketun, V. Tripkovic and J. K. Norskov, *Chem. Phys. Lett.*, 2008, **466**, 68–71.
35 F. Costanzo, M. Sulpizi, R. G. Della Valle and M. Sprik, *J. Chem. Phys.*, 2011, **134**, 244058.
36 H. Jiang, *J. Phys. Chem. C*, 2012, **116**, 7664–7671.
37 M. Grätzel, *Nature*, 2001, **414**, 338–344.
38 M. Gajdoš, K. Hummer, G. Kresse, J. Furthmüller and F. Bechstedt, *Phys. Rev. B: Condens. Matter*, 2006, **73**, 045112.
39 A. Antons, J. Neaton, K. M. Rabe and D. Vanderbilt, *Phys. Rev. B: Condens. Matter*, 2005, **71**, 024102.
40 J. H. Lee and A. Selloni, *Phys. Rev. Lett.*, 2014, **112**, 196102.
41 N. C. Bristowe, P. B. Littlewood and E. Artacho, *Phys. Rev. B: Condens. Matter*, 2011, **83**, 205405.
42 C. Cancellieri, D. Fontaine, S. Gariglio, N. Reyren, A. D. Caviglia, A. Fete, S. J. Leake, S. A. Pauli, P. R. Willmott, M. Stengel, P. Ghosez and J. M. Triscone, *Phys. Rev. Lett.*, 2011, **107**, 056102.
43 C. Cancellieri, N. Reyren, S. Gariglio, A. D. Caviglia, A. Fete and J. M. Triscone, *Europhys. Lett.*, 2010, **91**, 17004.
44 A. Caviglia, S. Gariglio, N. Reyren, D. Jaccard, T. Schneider, M. Gabay, S. Thiel, G. Hammerl, J. Mannhart and J.-M. Triscone, *Nature*, 2008, **456**, 624–627.
45 C. Cen, S. Thiel, G. Hammerl, C. W. Schneider, K. E. Andersen, C. S. Hellberg, J. Mannhart and J. Levy, *Nat. Mater.*, 2008, **7**, 298–302.
46 H. Chen, A. M. Kolpak and S. Ismail-Beigi, *Adv. Mater.*, 2010, **22**, 2881–2899.
47 G. Herranz, M. Basletic, M. Bibes, C. Carrétéro, E. Tafra, E. Jacquet, K. Bouzehouane, C. Deranlot, A. Hamzic, J.-M. Broto, A. Barthélémy and A. Fert, *Phys. Rev. Lett.*, 2007, **98**, 216803.

 This journal is © The Royal Society of Chemistry 2016

48 M. Huijben, G. Rijnders, D. H. A. Blank, S. Bals, S. V. Aert, J. Verbeeck, G. V. Tendeloo, A. Brinkman and H. Hilgenkamp, *Nat. Mater.*, 2006, **5**, 556–560.

49 H. Y. Hwang, Y. Iwasa, M. Kawasaki, B. Keimer, N. Nagaosa and Y. Tokura, *Nat. Mater.*, 2012, **11**, 103–113.

50 J. Lee and A. A. Demkov, *Phys. Rev. B: Condens. Matter*, 2008, **78**, 193104–193104.

51 H. X. Liang, L. Cheng, X. F. Zhai, N. Pan, H. L. Guo, J. Zhao, H. Zhang, L. Li, X. Q. Zhang, X. P. Wang, C. G. Zeng, Z. Y. Zhang and J. G. Hou, *Sci. Rep.*, 2013, **3**, 1975.

52 N. Nakagawa, H. Y. Hwang and D. A. Muller, *Nat. Mater.*, 2006, **5**, 204–209.

53 S. A. Pauli, S. J. Leake, B. Delley, M. Bjoerck, C. W. Schneider, C. M. Schlepuetz, D. Martoccia, S. Paetel, J. Mannhart and P. R. Willmott, *Phys. Rev. Lett.*, 2011, 106.

54 R. Pentcheva and W. E. Pickett, *Phys. Rev. Lett.*, 2009, **102**, 107602.

55 Z. S. Popovic, S. Satpathy and R. M. Martin, *Phys. Rev. Lett.*, 2008, **101**, 256801–256804.

56 L. Qiao, T. C. Droubay, T. C. Kaspar, P. V. Sushko and S. A. Chambers, *Surf. Sci.*, 2011, **605**, 1381–1387.

57 M. L. Reinle-Schmitt, C. Cancellieri, D. Li, D. Fontaine, M. Medarde, E. Pomjakushina, C. W. Schneider, S. Gariglio, P. Ghosez, J. M. Triscone and P. R. Willmott, *Nat. Commun.*, 2012, **3**, 932.

58 D. G. Schlom and J. Mannhart, *Nat. Mater.*, 2011, **10**, 168–169.

59 W. Siemons, G. Koster, H. Yamamoto, W. A. Harrison, G. Lucovsky, T. H. Geballe, D. H. A. Blank and M. R. Beasley, *Phys. Rev. Lett.*, 2007, **98**, 196802.

60 G. Singh-Bhalla, C. Bell, J. Ravichandran, W. Siemons, Y. Hikita, S. Salahuddin, A. F. Hebard, H. Y. Hwang and R. Ramesh, *Nat. Phys.*, 2011, **7**, 80–86.

61 S. Thiel, G. Hammerl, A. Schmehl, C. W. Schneider and J. Mannhart, *Science*, 2006, **313**, 1942–1945.

62 P. R. Willmott, S. A. Pauli, R. Herger, C. M. Schlepütz, D. Martoccia, B. D. Patterson, B. Delley, R. Clarke, D. Kumah, C. Cionca and Y. Yacoby, *Phys. Rev. Lett.*, 2007, **99**, 155502.

63 N. C. Bristowe, P. Ghosez, P. B. Littlewood and E. Artacho, *J. Phys.: Condens. Matter*, 2014, **26**, 143201.

64 X. Li, Z. Li and J. Yang, *Phys. Rev. Lett.*, 2014, **112**, 018301.

65 M. Anpo and M. Takeuchi, *J. Catal.*, 2003, **216**, 505–516.

66 R. J. Kennedy and P. A. Stampe, *J. Cryst. Growth*, 2003, **252**, 333–342.

67 X. Gong and A. Selloni, *J. Phys. Chem. B*, 2005, **109**, 19560–19562.

68 T. Basey-Fisher, S. Hanham, H. Andresen, S. Maier, M. Stevens, N. Alford and N. Klein, *Appl. Phys. Lett.*, 2011, **99**, 233703.

69 J. Moser, A. Barreiro and A. Bachtold, *Appl. Phys. Lett.*, 2007, **91**, 163513.

70 G. Kresse and J. Furthmüller, *Phys. Rev. B: Condens. Matter*, 1996, **54**, 11169.

71 P. E. Blöchl, *Phys. Rev. B: Condens. Matter*, 1994, **50**, 17953.

72 J. P. Perdew, J. Chevary, S. Vosko, K. A. Jackson, M. R. Pederson, D. Singh and C. Fiolhais, *Phys. Rev. B: Condens. Matter*, 1992, **46**, 6671.

73 N. A. Deskins and M. Dupuis, *Phys. Rev. B: Condens. Matter*, 2007, **75**, 195212.

74 N. A. Hill, *Annu. Rev. Mater. Res.*, 2002, **32**, 1–37.

75 J. Heyd, G. E. Scuseria and M. Ernzerhof, *J. Chem. Phys.*, 2003, **118**, 8207–8215.

76 J. Kang, S. Tongay, J. Zhou, J. Li and J. Wu, *Appl. Phys. Lett.*, 2013, **102**, 012111.

77 L. Bengtsson, *Phys. Rev. B: Condens. Matter*, 1999, **59**, 12301.